DOI: 10.1002/ejic.201001096

Electronic Band Structure, Optical Properties, and Photocatalytic Hydrogen Production of Barium Niobium Phosphate Compounds ($BaO–Nb_2O_5–P_2O_5$)

In Sun Cho,[a,b] Dong Wook Kim,[b] Dong Hoe Kim,[b] Seong Sik Shin,[b] Tae Hoon Noh,[b] Dong Wan Kim,*[c] and Kug Sun Hong*[b]

Keywords: Solid-phase synthesis / Ceramics / Electronic structure / Luminescence / Water splitting

Barium niobium phosphate compounds ($BaNb_2P_2O_{11}$ and $Ba_3Nb_2P_4O_{18}$), with corner-sharing NbO_6 octahedra as well as PO_4 tetrahedra, were prepared by a conventional solid-state reaction method, and their optical properties, electronic band structure, and photocatalytic activity were investigated. The powders were characterized by X-ray powder diffraction (XRD), field-emission SEM (FESEM), high-resolution TEM (HRTEM), and UV/Vis and fluorescence spectroscopy. Both compounds exhibit similar optical band gaps, 3.55 eV for $BaNb_2P_2O_{11}$ and 3.58 eV for $Ba_3Nb_2P_4O_{18}$. However, photoluminescence spectra revealed that a radiative recombination process of charge carriers is dominant in $Ba_3Nb_2P_4O_{18}$ (strong blue-white emission at 300 K) under UV irradiation, whereas no obvious emission was observed from $BaNb_2P_2O_{11}$. The photocatalytic activity for the evolution of H_2 from the splitting of pure water was evaluated. $BaNb_2P_2O_{11}$, which has a smaller photon emission at room temperature, exhibited a much higher photocatalytic activity than $Ba_3Nb_2P_4O_{18}$. The difference in the photocatalytic activity of the two compounds is attributed to their different electronic band structures, resulting from their different crystal-structure environments.

Introduction

In recent years, photocatalysis using solar energy has attracted considerable attention, because it is considered to be a promising "green" technology that can provide renewable energy as well as solve environmental problems.[1,2] The photocatalytic splitting of water using oxide semiconductors under light irradiation has received much attention in the quest to produce clean hydrogen from water cleavage. Extensive studies have been conduced in an attempt to develop efficient photocatalysts that can split water into hydrogen and oxygen. Among the photocatalysts, however, phosphate-based compounds that operate under the irradiation of UV or visible light have been rarely reported and are still limited.[3,4]

Titanium-, niobium-, and tantalum-based wide band-gap semiconductors have proven to be effective photocatalysts due to their special structure, in which a layered crystal structure composed of MO_6 (M = Ti, Nb, Ta) octahedra is formed, and the fairly high energy level of the metal d orbitals, which could be beneficial for the production of H_2 gas from water splitting.[2,5–8]

The crystal structures of $BaNb_2P_2O_{11}$ and $Ba_3Nb_2P_4O_{18}$ have been individually reported by Murashova et al.[9] and Wang et al.[10] Both compounds contain corner-sharing NbO_6 octahedra as well as PO_4 tetrahedra. In the structure of $BaNb_2P_2O_{11}$, each NbO_6 octahedron shares its corner oxygen atoms with three NbO_6 octahedra and three PO_4 tetrahedra. Conversely, $Ba_3Nb_2P_4O_{18}$ is composed of NbO_6 octahedra connected to five PO_4 tetrahedra. The crystal-structure parameters are listed in detail in Table 1. Our group recently reported the densification behavior and microwave dielectric properties of these two compounds.[11] However, there have been no reports on their optical, photophysical, and photocatalytic properties.

Table 1. Crystal structure parameters of BNP122 and BNP324.

Compound	Crystal system	Unit cell parameters					
		a [Å]	b [Å]	c [Å]	α [°]	β [°]	γ [°]
BNP 122	trigonal ($R\bar{3}c$)	5.072	5.072	59.1	90	90	120
BNP 324	triclinic ($P\bar{1}$)	4.8898	9.076	9.521	88.82	78.64	78.49

In this study, two barium niobium phosphate compounds, $BaNb_2P_2O_{11}$ (BNP122) and $Ba_3Nb_2P_4O_{18}$ (BNP324), were prepared by a conventional solid-state reaction, and their optical properties, electronic band structure, and photocatalytic activity for the evolution of H_2

[a] Department of Mechanical Engineering, Stanford University, Stanford, California 94305, USA
[b] Department of Materials Science and Engineering, Seoul National University,
Sillim-dong, Gwanak-gu, Seoul, South Korea
Fax: +82-2-886-4156
E-mail: kshongss@plaza.snu.ac.kr
[c] Department of Materials Science & Engineering, Ajou University,
Suwon 443-749, South Korea
E-mail: dwkim@ajou.ac.kr
Supporting information for this article is available on the WWW under http://dx.doi.org/10.1002/ejic.201001096.

from pure water under UV irradiation were investigated. In this way, the differences in their photocatalytic activity were elucidated from their crystal-structure environment and electronic band structure.

Results and Discussion

Crystal Structure and Powder Morphology

Figure 1 shows the XRD patterns of BNP122 and BNP324 powders prepared by a solid-state reaction method. Both powders exhibited single phases, and all of the reflection peaks were clearly indexed as the trigonal phase (JCPDS No. 40-0107) for BNP122 and triclinic phase (ICSD No. 90878) for BNP324.

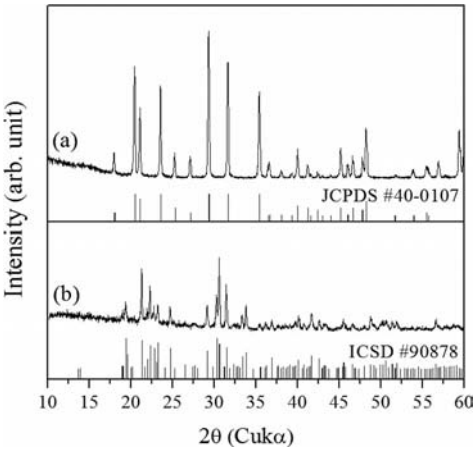

Figure 1. XRD patterns of (a) BNP122 and (b) BNP324 powders prepared at 1200 °C and 1100 °C, respectively.

Typical TEM images of the two powders are shown in Figure 2(a) and (d). The BNP122 powder exhibited a larger, irregular, and spherical morphology with an average size of 3 μm, whereas the BNP324 powder exhibited an anisotropic, faceted rod-like morphology with a size range of 0.5–3 μm. Both powders contained broken pieces resulting from the mechanical milling process (Figure S1). Figure 2(b) and (c) show an HRTEM image and the corresponding selected-area electron diffraction (SAED) pattern on a single particle of BNP122, respectively. The SAED pattern indexed to the [001] zone axis of the single particle and the HRTEM image shows lattice fringes with a width of 0.51 nm, corresponding to the (100) or (010) plane of trigonal BNP122.

For BNP324, the SAED pattern [Figure 2(f)] indexed to the [0–21] zone axis and the HRTEM image [Figure 2(e)] shows lattice fringes with widths of 0.47 and 0.41 nm, which correspond to the (100) and (012) planes, respectively, of triclinic BNP324. Moreover, the interplanar spacing of the lattice fringes along the length of the rods is 0.36 nm, which corresponds to the interplanar spacing of the (112) plane. Therefore, the anisotropic growth direction of BNP324 particles is considered to be in the [112] direction. The BET surface area measurements showed that the BNP122 powder had a smaller surface area (1.14 m^2/g) than the BNP324 powder (5.01 m^2/g), which is consistent with the FESEM results (Figure S1).

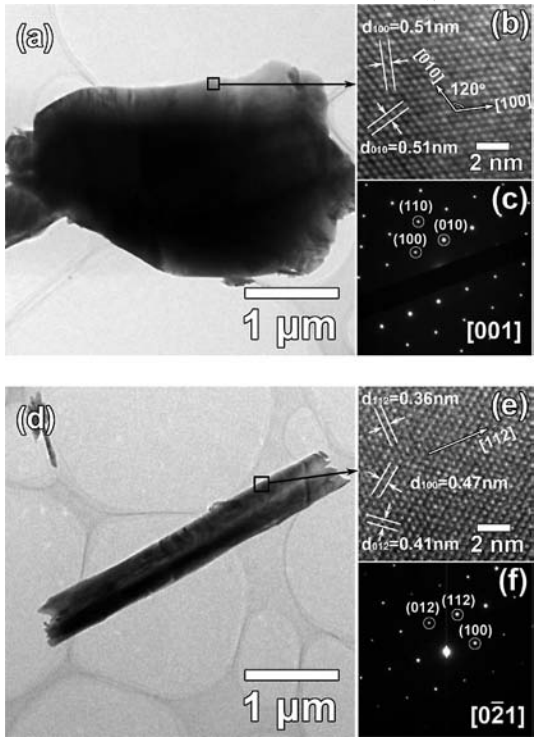

Figure 2. TEM, HRTEM images, and corresponding SAED patterns of (a)–(c) BNP122 and (d)–(f) BNP324 powders. [001] and [0–21] zone axes in (c) and (f), respectively, were identified.

Optical Properties and Electronic Band Structure

Figure 3(a) shows the diffuse-reflectance spectra of the BNP122 and BNP324 powders. Both powders exhibited a similar absorption band in the UV/Vis region, i.e. the absorption edges were 350 and 346 nm for BNP122 and BNP324, respectively.

The estimated band gap of BNP122 (3.55 eV) was slightly smaller than that of BNP324 (3.58 eV). Figure 3(b) shows the excitation and emission spectra of both powders at 300 K.

BNP324 exhibited a strong blue-white emission when excited at wavelengths less than 300 nm, whereas only a very weak emission peak was observed for BNP122 at 480 nm.

This result indicates that the recombination process of the excited charge carriers, especially radiative recombination (photon emission), is dominant in BNP324 when it is irradiated by UV light, i.e. almost all of the excited charge carriers recombine with each other, leading to a strong photon emission.

The crystal structures of BNP122 and BNP324 were constructed from published data (Figure 4).[9,10] In these two compounds, both NbO_6 octahedra and PO_4 tetrahedra coexist. However, their connection schemes are quite different, i.e. BNP122 has a layered structure, and BNP324 has a chain structure along the *a*-axis.

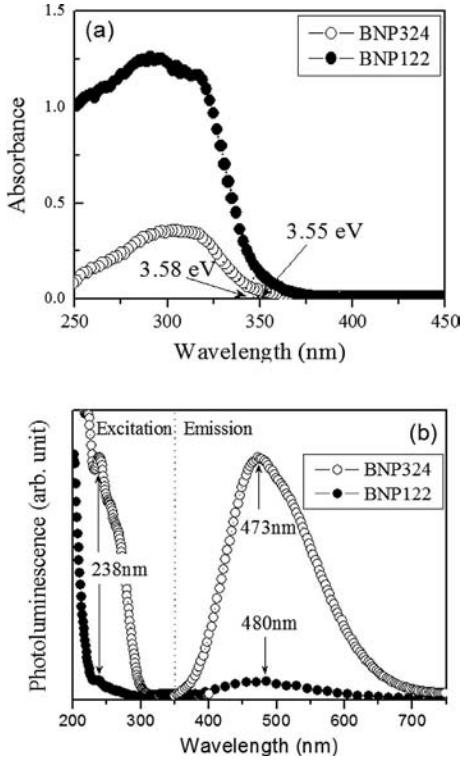

Figure 3. (a) UV/Vis diffuse reflectance spectra and (b) photoluminescence spectra of BNP122 and BNP324 powders at 300 K.

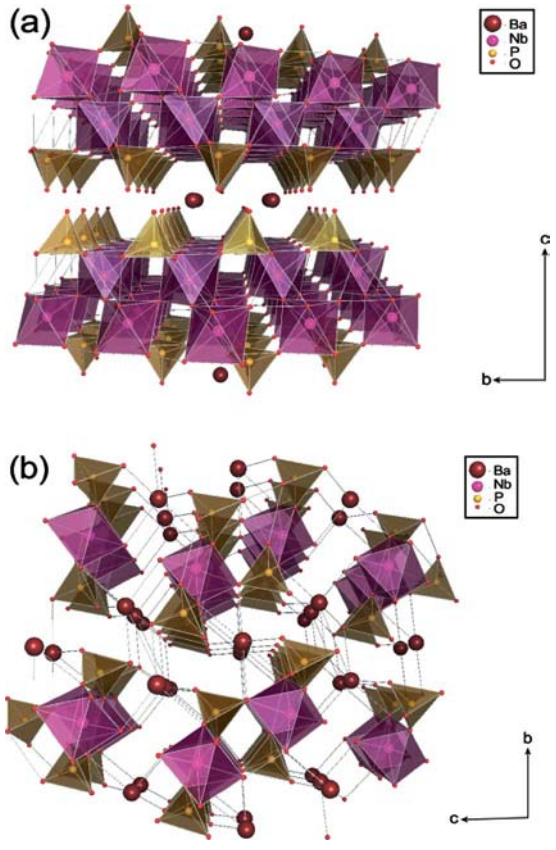

Figure 4. Perspective view of the crystal structures of (a) BNP122 (layered structure along the *c*-axis) and (b) BNP324 (chain structure along the *a*-axis).

The effect of the different crystal structures on the electronic band structures of the two compounds was investigated by DFT. Figure 5 shows the band structures and density of states (DOS) of trigonal BNP122 and triclinic BNP324.

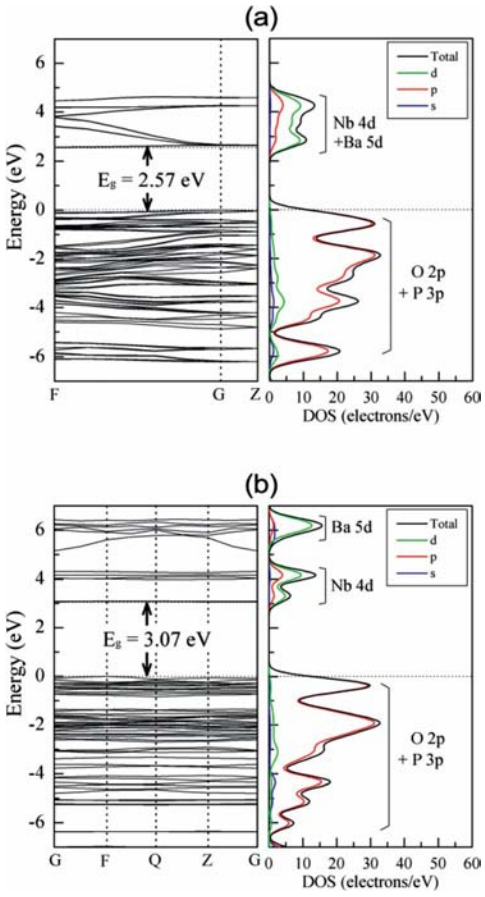

Figure 5. Electronic band structures and DOS of (a) BNP122 and (b) BNP324.

The calculated band gap of BNP122 (2.57 eV) is smaller than that of BNP324 (3.07 eV), which is in agreement with the tendency estimated from the absorption edges. In both compounds, moreover, the valence band comprises the O 2p and P 3p orbitals.

In the construction of the conduction band, the Nb 4d and Ba 5d orbitals are hybridized in BNP122. In constrast, these two orbitals are split in BNP324 and form two distinct additional bands between the valence and conduction bands. From the bond valence theory calculation,[11–13] the average bond strength of the Nb–O and P–O bonds in both compounds is similar, whereas that of the Ba–O bonds is quite different. The average strength of the Ba–O bonds in BNP324 (indicated by shorter bonds) is much higher than that of BNP122, which indicates the possibility of strong interactions between the Ba 5d orbital and the O 2p orbital. The band splitting is considered to be related to the strong interaction between the Ba 5d and O 2p orbitals resulting from the higher Ba–O bond strength.[14]

According to Blasse et al., self-luminescence properties in niobate compounds originate from charge transfer in the

MO_6 (M = W and Nb) octahedra.[15] Similarly, the strong luminescence in BNP324 (with intensity and emission wavelength comparable to those of $CaNb_2O_6$) is also considered to originate from the NbO_6 group, which induces additional sub-bands below the conduction band.

Photocatalytic Activity

The photocatalytic activities of BNP122 and BNP324 were evaluated by comparing their effect on the evolution of H_2 from pure water under UV irradiation. Figure 6(a) shows the obvious evolution of H_2 for BNP122, whereas H_2 evolution for BNP324 was barely detectable, in spite of its larger surface area.

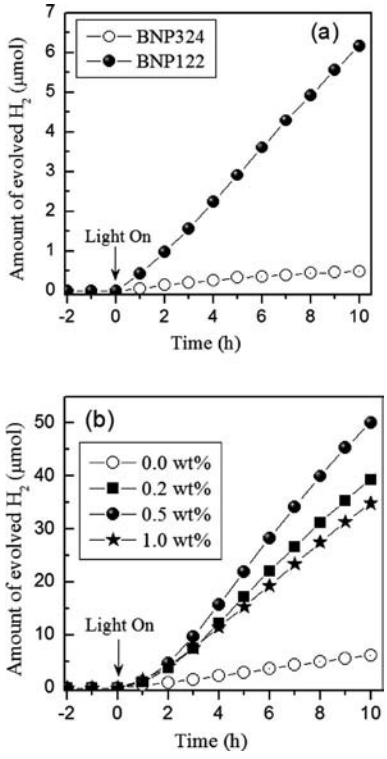

Figure 6. (a) Comparison of photocatalytic activity between BNP122 and BNP324 for H_2 evolution from pure water under UV light irradiation; (b) effect of cocatalyst (NiO_x) on the photocatalytic activity of BNP122.

Generally, the most important factors that affect the photocatalytic activity of a powder photocatalyst are its optical absorption capability (optical band gap), surface area, and the separation/diffusion rate of the photogenerated charge carriers (mobility).[1,7,16–20] A smaller band gap is more effective in generating charge carriers, and a higher surface area provides a larger number of active sites on the surface, allowing more water molecules to be adsorbed. Moreover, the higher mobilities of the charge carriers indicate that there is a higher probability of transferring the photogenerated charge carriers from the bulk to the surface, i.e. more charge carriers can participate in the photocatalytic reaction. As discussed above, the UV-excited charge carriers in BNP324 were mostly consumed by photon emission, whereas those in BNP122 were not. Therefore, the higher photocatalytic activity of BNP122, despite its smaller surface area, can be mainly attributed to its smaller photon emission, i.e. the higher separation/diffusion rate of the charge carriers, due to its unique layered crystal structure.[21]

After the photocatalytic reactions, both powders were rechecked by XRD and FESEM (Figures S2 and S3). No changes in their crystal structures or morphologies were detected, indicating the stability of the powders against UV irradiation.

The photocatalytic activity of BNP122 was further investigated by loading it with cocatalysts. There was no significant morphology change after cocatalyst loading (Figure S4). Figure 6(b) shows the effects of the NiO_x cocatalyst on the H_2 evolution rate. It was found that the photocatalytic activity of BNP122 was greatly enhanced by the NiO_x cocatalyst loading and that the optimum loading was 0.5 wt.-%. Moreover, the stoichiometric evolution of H_2 and O_2 was checked for all the samples (Figure S5). The photocatalytic activities of BNP122 and BNP324 for the evolution of H_2 and O_2 from pure water are summarized in Table 2. It is considered that the enhanced photocatalytic activity afforded by the NiO_x cocatalyst loading is related to the efficient charge separation caused by the minimization of the bulk recombination.[22] The NiO_x cocatalyst is more effective than Pt as cocatalyst in enhancing the photocatalytic activity of BNP122.

Table 2. Photocatalytic H_2 and O_2 evolution rate from pure water by using BNP122 and BNP324 with cocatalysts under UV irradiation.

Compound	Cocatalyst	Cocatalyst loading [wt.-%]	Activity [μmol/gh]	
			H_2	O_2
BNP122	none	0	2.1	1.2
	NiO_x	0.2	13.1	6.9
		0.5	16.7	7.9
		1.0	11.6	6.2
		1.5	11.2	6.7
	Pt	0.5	7.1	3.8
BNP324	none	0	0.1	–
	NiO_x	1.0	0.2	0.1

Conclusions

The barium niobium phosphate compounds $BaNb_2P_2O_{11}$ (BNP122) and $Ba_3Nb_2P_4O_{18}$ (BNP324) with corner-sharing NbO_6 octahedra and PO_4 tetrahedra were prepared by a conventional solid-state reaction method, and their electronic band structure, optical properties, and photocatalytic activity were investigated.

Both compounds have similar optical band gaps (ca. 3.6 eV). Compared with BNP122, however, BNP324 exhibited a higher photoluminescence intensity at room temperature under UV irradiation, indicating that it has a higher radiative recombination rate of UV-excited charge carriers. From the electronic band structure calculation, it has been inferred that the strong photon emission of BNP324 at

room temperature is related to the splitting of the conduction band, due to the shorter Ba–O bond. Although BNP122 has a smaller surface area than BNP324, it exhibited a higher photocatalytic activity for the evolution of H_2 from water, and its photocatalytic activity was enhanced by loading it with an NiO_x cocatalyst.

Experimental Section

Preparation of Powders: $BaNb_2P_2O_{11}$ and $Ba_3Nb_2P_4O_{18}$ were prepared by a conventional solid-state reaction method. $BaCO_3$, Nb_2O_5 (High Purity Chemicals, 99.9%, Japan), and $(NH_4)_2HPO_4$ (Junsei Chemicals, 99%, Japan) were used as the raw materials. Stoichiometric mixtures of the starting materials were homogenized by ball milling with zirconia media for 24 h using absolute ethanol (99.9%), and the mixtures were rapidly dried, then calcined at 1100 or 1200 °C in air for 4 h with a heating rate of 5 °C/min. After the calcination process, the obtained powders were milled again for 6 h by using absolute ethanol.

Measurements and Characterizations: The crystal structures and phase purity of the powders were determined by using XRD (M18XHF, Mac-science). The powder morphologies and microstructures were investigated by using FESEM (JSM-6330F, JEOL) and TEM (JEM-3000F, JEOL). The UV/Vis diffuse-reflectance spectra were obtained by using UV/Vis/NIR spectroscopy (U-4001, Hitachi), and the photoluminescence spectra were obtained by fluorescence spectroscopy (LS 55, Perkin–Elmer) at room temperature. The specific surface areas of the powders were measured with a Brunauer–Emmett–Teller (BET) surface-area analyzer (BELSORP-mini II, BEL). The band-structure calculation based on plane wave DFT was performed by using the CASTEP program.[23] The convergence criteria applied were 1×10^{-6} eV for the total energy change per atom. The gradient corrections were performed by the generalized gradient approximation using Perdew–Burke–Ernzerhof functionals and ultrasoft pesudopotentials.

Photocatalytic Reactions: The photocatalytic reactions for H_2 or O_2 evolution were conducted at room temperature in a closed gas circulation system with an outer-irradiation-type quartz reactor (200 mL). A 450 W high-pressure mercury lamp was used as the UV light source. It was positioned inside a cylindrical vessel surrounded by a circulating water jacket, which was used to cool the lamp. The distance between the reactor and the lamp was 15 cm. The photocatalyst powder (0.3 g) was dispersed in distilled water (150 mL) by magnetic stirring after sonication (10 min). Before irradiation, the closed gas circulation system and the reactor were degassed with high-purity Ar gas (99.999%). The amount of H_2 or O_2 evolved was determined by using gas chromatography (Donam, DS6200, Korea). The Pt cocatalyst was loaded on the surface of the powder samples by an in situ photodeposition method using an aqueous $H_2PtCl_6 \cdot 6H_2O$ solution. The NiO_x cocatalysts were loaded by an impregnation method using an $Ni(NO_3)_2$ ethanol solution. The NiO_x-loaded powders were reduced by an H_2 (5%)/N_2 (95%) gas (300 sccm) at 500 °C for 2 h and subsequently oxidized by O_2 (20 sccm) at 350 °C for 2 h [sccm = standard cubic centimeters per minute (cm^3/min)].

Supporting Information (see footnote on the first page of this article): Additional XRD, FESEM images, and stoichiometric H_2 and O_2 evolution results.

Acknowledgments

This work was supported by a National Research Foundation of Korea (NRF) grant funded by the Korea government (MEST) (No. 2009-0092779) and by the Priority Research Centers Program through the NRF funded by the Ministry of Education, Science and Technology (2010-0029617).

[1] M. R. Hoffmann, S. T. Martin, W. Choi, D. W. Bahnemann, *Chem. Rev.* **1995**, *95*, 69.
[2] A. Fujishima, K. Honda, *Nature* **1972**, *238*, 37.
[3] Y. Yang, Y. Murakami, A. Y. Nosaka, Y. Nosaka, *AZojomo* **2008**, 4, 1.
[4] Z. Yi, J. Ye, N. Kikugawa, T. Kako, S. Ouyang, H. Stuart-Williams, H. Yang, J. Cao, W. Luo, Z. Li, Y. Liu, R. L. Withers, *Nat. Mater.* **2010**, *9*, 559.
[5] K. Domen, J. N. Kondo, M. Hara, T. Takata, *Bull. Chem. Soc. Jpn.* **2000**, *73*, 1307.
[6] D. W. Hwang, H. G. Kim, J. Kim, K. Y. Cha, Y. G. Kim, J. S. Lee, *J. Catal.* **2000**, *193*, 40.
[7] A. Kudo, H. Kato, J. Nakagawa, *J. Phys. Chem. B* **2000**, *104*, 571.
[8] H. Kato, A. Kudo, *Catal. Lett.* **1999**, *58*, 153.
[9] E. V. Murashova, V. K. Trunov, Y. A. Velikodnyi, *Russ. J. Inorg. Chem.* **1986**, *31*, 951.
[10] X. Wang, L. Liu, A. J. Jacobson, *J. Mater. Chem.* **2000**, *10*, 2774.
[11] I. S. Cho, J. S. Lee, S. T. Bae, J. R. Kim, K. S. Hong, *J. Electroceram.* **2009**, *23*, 154.
[12] I. D. Brown, *Acta Crystallogr., Sect. B* **1992**, *48*, 553.
[13] I. D. Brown, R. D. Shannon, *Acta Crystallogr., Sect. A* **1973**, *29*, 266.
[14] M. W. Stoltzfus, P. M. Woodward, R. Seshadri, J. H. Klepeis, B. Bursten, *Inorg. Chem.* **2007**, *46*, 3839.
[15] G. Blasse, *J. Solid State Chem.* **1988**, *72*, 72.
[16] J. M. Herrmann, *Catal. Today* **1999**, *53*, 115.
[17] K. Maeda, K. Domen, *J. Phys. Chem. C* **2007**, *111*, 7851.
[18] R. Asahi, T. Morikawa, T. Ohwaki, K. Aoki, Y. Taga, *Science* **2001**, *293*, 269.
[19] I. S. Cho, S. T. Bae, D. K. Yim, D. W. Kim, K. S. Hong, *J. Am. Ceram. Soc.* **2009**, *92*, 506.
[20] O. C. Compton, E. C. Carroll, J. Y. Kim, D. S. Larsen, F. E. Osterloh, *J. Phys. Chem. C* **2007**, *111*, 14589.
[21] M. Machida, J. Yabunaka, T. Kijima, *Chem. Mater.* **2000**, *12*, 812.
[22] L. W. Zhang, H. B. Fu, Y. F. Zhu, *Adv. Funct. Mater.* **2008**, *18*, 2180.
[23] M. C. Payne, M. P. Teter, D. C. Allan, T. A. Arias, J. D. Joannopoulos, *Rev. Mod. Phys.* **1992**, *64*, 1045.

Received: October 15, 2010
Published Online: March 30, 2011

